Am J Physiol Cell Physiol 290: C832–C843, 2006.
First published October 26, 2005; doi:10.1152/ajpcell.00405.2005.

Bipolar assembly of caveolae in retinal pigment epithelium

Rosalia C. Mora,[1] Vera L. Bonilha,[2] Bo-Chul Shin,[3] Jane Hu,[4] Leona Cohen-Gould,[5] Dean Bok,[6] and Enrique Rodriguez-Boulan[1]

[1]*M. Dyson Vision Research Institute, Department of Ophthalmology, Weill Medical College of Cornell University, New York;* [2]*The Cole Eye Institute, The Cleveland Clinic Foundation, Cleveland, Ohio;* [3]*Department of Pediatrics and* [4]*Department of Ophthalmology, David Geffen School of Medicine, University of California, Los Angeles;* [5]*Departments of Biochemistry and Cell and Developmental Biology, Weill Medical College of Cornell University, New York, New York; and* [6]*Jules Stein Eye Institute, Brain Research Institute, and Department of Neurobiology, David Geffen School of Medicine, University of California, Los Angeles, California*

Submitted 11 August 2005; accepted in final form 15 October 2005

Mora, Rosalia C., Vera L. Bonilha, Bo-Chul Shin, Jane Hu, Leona Cohen-Gould, Dean Bok, and Enrique Rodriguez-Boulan. Bipolar assembly of caveolae in retinal pigment epithelium. *Am J Physiol Cell Physiol* 290: C832–C843, 2006. First published October 26, 2005; doi:10.1152/ajpcell.00405.2005.—Caveolae and their associated structural proteins, the caveolins, are specialized plasmalemmal microdomains involved in endocytosis and compartmentalization of cell signaling. We examined the expression and distribution of caveolae and caveolins in retinal pigment epithelium (RPE), which plays key roles in retinal support, visual cycle, and acts as the main barrier between blood and retina. Electron microscopic observation of rat RPE, in situ primary cultures of rat and human RPE and a rat RPE cell line (RPE-J) demonstrated in all cases the presence of caveolae in both apical and basolateral domains of the plasma membrane. Caveolae were rare in RPE in situ but were frequent in primary RPE cultures and in RPE-J cells, which correlated with increased levels in the expression of caveolin-1 and -2. The bipolar distribution of caveolae in RPE is striking, as all other epithelial cells examined to date (liver, kidney, thyroid, and intestinal) assemble caveolae only at the basolateral side. This might be related to the nonpolar distribution of both caveolin-1 and 2 in RPE because caveolin-2 is basolateral and caveolin-1 nonpolar in other epithelial cells. The bipolar localization of plasmalemmal caveolae in RPE cells may reflect specialized roles in signaling and trafficking important for visual function.

caveolin; raft microdomains; membrane traffic; normal rat kidney

THE RETINAL PIGMENT EPITHELIUM (RPE) performs a variety of specialized transport and metabolic functions essential for vision. Thus the RPE acts as an active barrier between the choroidal vessels and the neural retina through membrane transporters that transfer blood metabolites to the subretinal space and retinal waste products to the bloodstream. The RPE also performs phagocytosis and digestion of old photoreceptor outer segments (3, 56). To carry out these functions, the RPE is highly polarized, like other epithelial cells. RPE cells exhibit reverse apical polarity of many proteins that are expressed basolaterally in other epithelia, e.g., Na^+-K^+-ATPase (13, 16), extracellular matrix metalloproteinase inducer (23), neural cell adhesion molecule (14), and lactate monocarboxylate transporter-1 (31). Furthermore, the RPE utilizes an indirect transcytotic route to target the apical protein influenza hemagglutinin (HA) from the Golgi complex to the apical plasmalemma (2), a process that in other epithelial cells occurs by direct transport between Golgi complex and apical surface (35). The mechanisms involved in differential targeting between RPE and other epithelia are largely unknown.

Caveolae, initially named plasmalemmal vesicles, were first described 50 years ago on the plasmalemma of endothelial cells, where they are very abundant (26). By thin-section electron microscopy, caveolae appear as omega-shaped, invaginated plasma membrane domains that are 55–90 nm in diameter. In contrast to the distinctive, thick electron-dense coat of clathrin-coated vesicles, caveolae are smooth surfaced. Caveolae are associated with the structural proteins caveolin-1 and -2 in most cells and with caveolin-3 in muscle cells (33, 36, 38, 40, 50). Caveolin-1 is expressed as alternatively spliced α- and β-isoforms (18). Caveolin-1 is primarily responsible for the assembly of caveolae as expression of this protein promotes the appearance of caveolae in lymphocytes (10), in Fischer rat thyroid (FRT) thyroid epithelial cell line (25) and in Caco 2 cells (49). However, recent studies (11, 19, 42) suggest that caveolin-2 enhances the efficiency of caveolar biogenesis in HepG2 and LNCaP cells. Moreover, the caveolin-1-dependent polarized morphogenesis of caveolae in Madin-Darby canine kidney (MDCK) cells (25, 49) appears to require the presence of both caveolin-1 and 2 (19). Thus, despite the nonpolar distribution of caveolin-1 in MDCK cells, caveolae are formed only on the basolateral plasmalemma, where caveolin-2 is localized and probably the hetero-oligomerization of caveolins-1 and -2 is necessary for the efficient basolateral morphogenesis of caveolae (19, 37). In FRT cells, hetero-oligomerization of caveolin-1 and -2 targets Golgi-localized caveolin-2 to the plasma membrane, renders caveolin-2 detergent insoluble in sedimentation assays, and translocates caveolin-2 to low-density microdomains in flotation assays (25). Similarly to MDCK, FRT cells also assemble polarized plasmalemmal caveolae (25).

Biophysical experiments in cultured fibroblastic and epithelial cells have shown that plasmalemmal caveolae are stationary and held in place by the cortical actin cytoskeleton underlying the plasma membrane; however, on interaction with specific ligands, e.g., the simian virus 40 (SV40), they may detach from the membrane and be internalized as endocytic vesicles (44), see Ref. 30 for a review.

Caveolae concentrate a variety of proteins and signaling molecules, e.g., glycosyl phosphatidylinositol-linked proteins,

Address for reprint requests and other correspondence: E. Rodriguez-Boulan, Dyson Vision Research Institute, LC300, Weill Medical College of Cornell Univ., 1300 York Ave., New York, NY 10021 (e-mail: boulan@med.cornell.edu).

The costs of publication of this article were defrayed in part by the payment of page charges. The article must therefore be hereby marked "*advertisement*" in accordance with 18 U.S.C. Section 1734 solely to indicate this fact.

endothelial nitric oxide synthase and growth factor receptors (22, 33, 52). Caveolae are preferred sites of extracellular Ca^{2+} entry in living cells and Ca^{2+} that enters through this portal stimulates nitric oxide production (17). Certain bacteria enter cells via a unique phagocytic route that uses caveolae as a source of membrane for internalization (39). Caveolin-1 interacts with many proteins and regulates the signaling of molecules, such as Src family tyrosine kinases, G proteins, and epidermal growth factor receptor (33, 53). Caveolin-1 might be also involved in the scaffolding of phototransduction proteins, as suggested by its association with a pool of transducin α-subunit (8) in lipid rafts isolated from rod outer segments (1, 8). Finally, caveolins are considered organizers and stabilizers of the so-called lipid raft microdomains and are presumed to have important functions in membrane trafficking (12, 37). Caveolin-1 was recently identified as a trafficking chaperone for GPI-anchored proteins (41), for angiotensin II type receptor (54), for caveolin-2 (25, 28) and for phosphofructokinase (47). During biosynthetic transport, certain classes of membrane proteins, such as influenza HA and GPI-anchored proteins, are incorporated at the Golgi complex into cholesterol/sphingolipid-rich detergent (Triton X-100)-insoluble raft membrane microdomains (6). Antibodies against caveolin-1 added to the cytoplasm block transport of the apical protein influenza HA but do not affect delivery of basolateral proteins (37). The association of caveolin-1 with rafts may therefore be important in directing the vectorial delivery of some apical proteins (35).

Herein, we report that RPE cells in situ (in the eye) and in culture display a bipolar localization of caveolae at the plasma membrane. This localization is strikingly different from that observed in liver, kidney, thyroid, and intestinal epithelia, where caveolae are assembled only at the basolateral membrane (4, 7, 19, 25, 49). RPE cells display a nonpolarized localization of both caveolin-1 and 2, a different scenario from that found in other epithelial cells, where caveolin-1 is nonpolarized and caveolin-2 is basolateral. Our results suggest that caveolins and caveolae may play important roles in the interaction between RPE and the neural retina.

MATERIALS AND METHODS

Materials

Cell culture reagents (Cellgro) were purchased from Mediatech (Herndon, VA) and chemicals from Sigma (St. Louis, MO), unless otherwise specified. Antibodies and their sources were as follows: a polyclonal antibody (pAb) to caveolin-1 and a monoclonal antibody (mAb) to caveolin-2 (clone 65), were purchased from BD Biosciences Transduction Laboratories (San Diego, CA). A rabbit antibody to caveolin-2 was purchased from Affinity BioReagents (Golden, CO). A guinea pig antibody to glucose transporter GLUT1 was kindly provided by K. Takata (Gunma University Medical School, Japan). Fluorochrome (Alexa)-conjugated secondary anti-guinea pig, anti-mouse, and anti-rabbit antibodies were all from Molecular Probes (Eugene, OR). The caveolin-1 cDNA was provided by R. G. W. Anderson (University of Texas, Southwestern, Dallas, TX). The caveolin-2 and myc-tagged caveolin-1 cDNAs were provided by M. Lisanti (Albert Einstein College of Medicine, Bronx, NY).

Cell Culture

Cell lines used in the present study included RPE-J cells, MDCK, FRT, normal rat kidney (NRK-52E), and human colon adenocarcinoma (CaCo2) cells. The cells were maintained in Dulbecco's modified Eagle's medium (DMEM), supplemented with 5% (MDCK and NRK-52E) or 10% (CaCo2) fetal bovine serum. FRT cells were grown in Ham's F-12/Coon's modified medium (Sigma). Postconfluent (3–5 days) MDCK, FRT, and CaCo2 cells were used for all of the experiments. Cells were plated at a high density (300,000 cells/cm^2) on tissue culture dishes or polycarbonate Transwell R chambers (Corning Costar, Cambridge, MA). RPE-J cells were originally obtained from rat RPE by immortalization with temperature-sensitive SV40 T antigen; they were cultured at the permissive temperature of 32°C, as previously described (25a). RPE-J cells were grown in DMEM supplemented with 4% heat-inactivated (30 min at 56°C) CELLect Gold fetal calf serum (ICN Biomedicals; Irvine, CA), glutamine, nonessential amino acids, and penicillin/streptomycin. To obtain a differentiated epithelial phenotype, the cells were plated on polycarbonate filters (Corning Costar) coated with a thin layer of Matrigel (Collaborative Research, Bedford, MA), cultured in growth medium supplemented with 10^{-8} M retinoic acid for 6–7 days, and then switched to the nonpermissive temperature (39.5°C) for 36–48 h to block SV40 T antigen expression.

Transfection with Caveolin cDNAs

Full-length human caveolin-2 (either nontagged or myc tagged) and full-length human caveolin-1 cDNAs (either nontagged or myc tagged) were transfected in RPE-J, MDCK, and FRT cells, as previously described (25).

Primary rat RPE cultures were prepared from 3- to 4-wk-old Long Evans rats (Charles River Laboratories, Wilmington, MA). The animals were euthanized by CO_2 asphyxiation. After death, the eyes were enucleated and then stored in Hanks' balanced salt solution (HBSS) containing Ca^{2+}. After a circumferential incision was made above the ora serrata, the lens, iris, and vitreous body were removed. The eyecups with the neural retina exposed were incubated in 300 U/ml hyaluronidase in HBSS + Ca^{2+} for 1 h at 37°C. The neural retina was then peeled off from the RPE and the eyecups were incubated in 2 mg/ml trypsin (Difco Laboratories, Detroit, MI) in HBSS for 60 min at 37°C. The RPE sheets were teased from the underlying choroid with needles, collected, and incubated with 0.25% trypsin and 0.1% EDTA (CellGro) for 1 min. The cells were plated on Matrigel-coated Transwell filters and cultured without being passaged further in DMEM supplemented with 10% FCS, L-glutamine, nonessential amino acids, and antibiotics.

Human Fetal RPE Cultures

Cells were collected from the eyes of aborted human fetuses of 19 wk gestation. The fetal eyes were obtained from Advanced Bioscience Resources (Alameda, CA). The tenets of the Declaration of Helsinki were followed and donor approval was obtained, as was Institutional Human Experimentation Committee approval for the use of human eyes. The culture method for obtaining human RPE cells and their amplification in low-Ca^{2+} medium before their experimental use was performed as previously described (15). The cells were grown in Chee's essential replacement medium containing 1% bovine retinal extract. They were seeded onto mouse laminin-coated 12-mm-thick Millicell-PCF filters (Millipore, Bedford, MA) with a pore size of 0.4 μm and maintained for at least 2 mo in culture until they exhibited a high state of differentiation, as evidenced by heavy melanization and transepithelial resistances >500 Ω/cm^2.

Tissue Specimens

Fresh tissues (other than eyes) for use in immunoblot analyses were collected from CO_2 anesthetized adult Long-Evans rats after an intracardiac perfusion with HBSS; the tissue specimens (heart and brain) were stored at −80°C until needed.

Cryosections

The eyes of CO_2-anesthetized Long-Evans rats were enucleated and either frozen immediately in optimum cutting temperature compound (Tissue-Tek OCT, Miles Laboratories, Elkhart, IN) or fixed with 2–3% paraformaldehyde in phosphate-buffered saline (PBS) containing 0.5 mM $CaCl_2$ and 0.5 mM $MgCl_2$ (PBS/CM). Paraformaldehyde-fixed eyecups were infiltrated with 30% sucrose in PBS/CM and then with Tissue-Tek OCT. When it was necessary to maintain the RPE-neural retina interaction, the rats were anesthetized by CO_2 asphyxiation and subjected to intracardiac perfusion with HBSS, followed by 4% paraformaldehyde in PBS/CM. Perfusion-fixed eyes were enucleated, the corneas were incised, and then further immersion fixed for 1 h. Ten-micrometer-thick cryosections were cut on a cryostat (Bright Instrument) and collected on slides. Neural retinal-free RPE-choroid was obtained after removal of the neural retina after treatment of eye cups for 10 min at room temperature with 300 U/ml of hyaluronidase; the 10-μm-thick sections were prepared in a cryostat.

Immunohistochemistry

For immunofluorescence staining two different fixation protocols were used: *1*) 2–3% paraformaldehyde and *2*) organic solvent (methanol). Paraformaldehyde (15 min, 4°C) or ice-cold methanol (5 min) fixation were used for visualization of caveolins in cells or on cryosections, respectively.

Cryosections and cells fixed and permeabilized with methanol were first blocked for 30 min with 1% bovine serum albumin (BSA), 5% normal goat serum (Vector Laboratories; Burlingame, CA), 10 mM glycine in PBS (*buffer A*), and then incubated with antibodies in *buffer A*. Paraformaldehyde-fixed specimens were rinsed with PBS/CM three times, quenched in 25 mM NH_4Cl for 15 min, permeabilized for 15 min at 4°C with 0.1% saponin in PBS/CM containing 1% BSA, 5% normal goat serum, and 10 mM glycine (*buffer B*), and then incubated with antibodies in *buffer B*. Permeabilized specimens were incubated with primary antibodies for 4–10 h at 4°C, and, after being washed extensively, then incubated with secondary antibodies for 2–4 h at 4°C and washed again.

The fluorescent secondary antibodies were Alexa conjugated and highly cross-adsorbed goat anti-rabbit IgG (either Alexa 488 or Alexa 594), goat anti-mouse IgG (either Alexa 488 or Alexa 594), and goat anti-guinea pig IgG (Alexa 488). Controls included tests for interspecies cross-reactivity, as well as incubation with nonimmune rabbit IgG or nonimmune mouse IgG in lieu of primary antibodies or incubation only with the secondary antibodies. After immunostaining the specimens were incubated with 1:10,000 dilution in PBS from a 3 mM stock solution of 4′,6-diamidino-2-phenylindole (Molecular Probes) to stain cell nuclei (blue emission). The specimens were then mounted and fixed onto glass slides with the use of Vectashield mounting reagent (Vector Laboratories).

Cells and cryosections were analyzed with an epifluorescence microscope (model E-600, Nikon, Tokyo, Japan) or with a LSM 510 (Zeiss, Thornwood, NY) or TCS SP2 (Leica Microsystems) confocal microscope. On the Nikon epifluorescence microscope the images were acquired using a back-illuminated, cooled, charge-coupled device camera (CCD1000-PB, Princeton Instruments) and the appropriate filter cubes were obtained from Nikon. The digital images were transferred to a computer workstation running MetaMorph imaging software (Universal Imaging, West Chester, PA) and further processed with Photoshop 5 (Adobe Systems, San Jose, CA). Fluorescence intensity was quantified with the use of MetaMorph.

Western Blot Analysis

RPE tissues as well as cultured RPE and other epithelial cells were lysed for 60 min on ice in a buffer containing 10 mM Tris, 15 M NaCl, 5 mM EDTA, 1% Triton X-100, 60 mM octyl-glucoside, pH 8.0, and

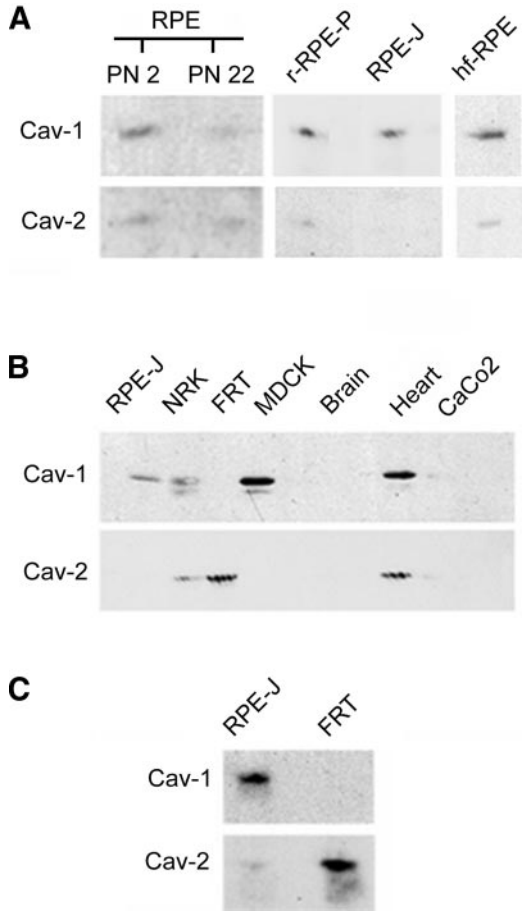

Fig. 1. Western blot analysis of the in vivo and in vitro expression of caveolins in retinal pigment epithelium (RPE). *A*: protein extracts of intact sheets of RPE from rat eyes of postnatal (PN) *day 2* and *22* were separated by SDS-PAGE (15%), transferred to nitrocellulose, and probed with antibodies to caveolin-1 (cav-1; pAb 13360) and caveolin-2 (cav-2; mAb 65). Note the expression of cav-1 and cav-2 in RPE from rat eyes, in rat primary RPE (rRPE-P) cells, as well as in fetal human (hf)-RPE (100 μg/lane of rat RPE tissue extracts and 50 μg/lane cell extracts). *B*: comparison of the expression level of caveolins in RPE-J and in several established cell lines. Tissue extracts from heart and brain were included as controls. Fifty micrograms of total cellular proteins extracted from immortalized cultured RPE-J cell line and from other cell types (as indicated) were resolved by SDS-PAGE (15%) and transferred to nitrocellulose. The membrane was blotted with antibodies to cav-1 and cav-2. *C*: Western blot analysis in higher amount of cell extracts loaded on SDS-PAGE (100 μg/lane of cell extracts) detected a low level of cav-2 in RPE-J cells. Proteins were visualized using a standard chemiluminescent system. In the amount of extract analyzed on the blots in *A* and *B* and using a standard chemiluminescent reagent kit, cav-2 was not detected in RPE-J cells (*A* and *B*) and was only barely detected in primary RPE (RPE-P) cells (*A*). The monoclonal antibody (mAb 65) is species specific: it detects cav-2 in rat cells but not in Madin-Darby canine kidney (MDCK) cells (*B*). NRK, normal rat kidney; FRT, Fischer rat thyroid.

subjected to centrifugation for 10 min at 14,000 rpm in a tabletop microcentrifuge. The protein content of the extracts was determined using a DC protein assay kit (Bio-Rad Laboratories, Hercules, CA) with BSA as a standard.

Alternatively, total protein extracts of RPE cells were prepared by directly lysing cells in SDS-PAGE sample buffer and after the samples were boiled for 5 min, protein content was determined with the use of a Coomassie Plus Protein Assay Reagent (Pierce Biotechnology, Rockford, IL). Equal amounts of protein (50 μg routinely and 100 μg occasionally) were analyzed by SDS-PAGE (15% acrylamide). After transfer to nitrocellulose, the blots were incubated for 1 h in 10 mM Tris·HCl, 150 mM NaCl, and 0.1% Tween 20, pH 8,

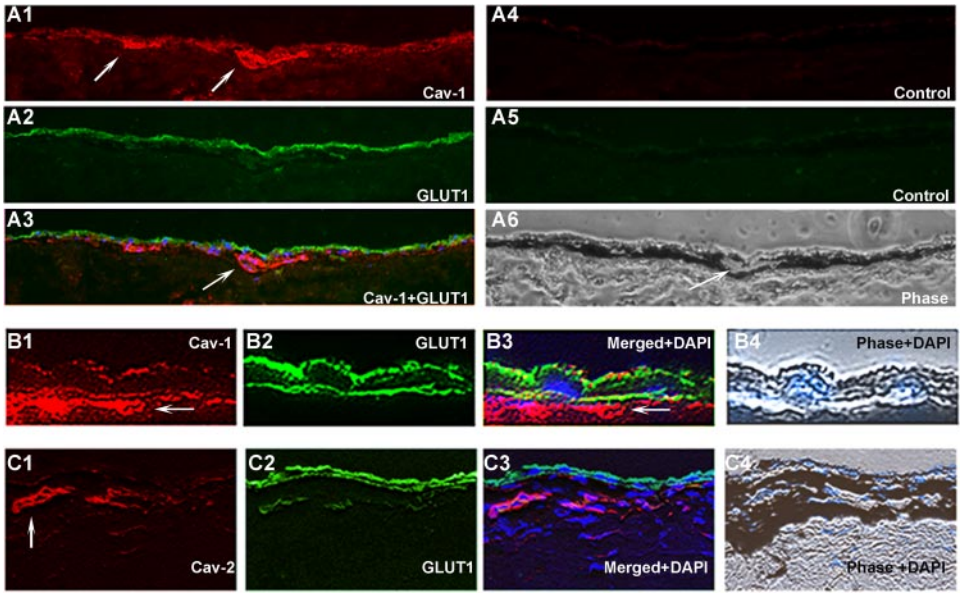

Fig. 2. Immunolocalization of cav-1 and -2 in the rat RPE. *A1–B4*: double immunofluorescence labeling of RPE-choroid frozen cross-sections was performed with cav-1 polyclonal antibody (*A1* and *B1*), with the monoclonal cav-2 antibody (C1) and the glucose transporter GLUT1 antibody (*A2*, *B2*, and *C2*). *A3*, *B3*, and *C3* are merged images of *A1* and *A2*, of *B1* and *B2*, and of *C1* and *C2*, respectively. Phase-contrast images of the immunostained fields are shown for reference in *A6*, *B4*, and *C4*. *A4* and *A5* are cryosections of the RPE-choroid complex incubated with normal rabbit serum in place of the primary antibody and examined in the red (*A4*) and green (*A5*) channel: no immunoreactivity was observed. Nuclei stained with 4′,6-diamidino-2-phenylindole (DAPI) are blue (*A3*, *B3*, *B4*, *C3*, and *C4*). Note in *A1* the presence of cav-1 in RPE is at a much lower level than in the blood vessels (arrows), and at a higher magnification in *B1*, the nonpolar distribution of cav-1. The immunostaining of cav-2 was below the detection limits of the monoclonal antibody used (C1–C3). Arrows point to blood vessels.

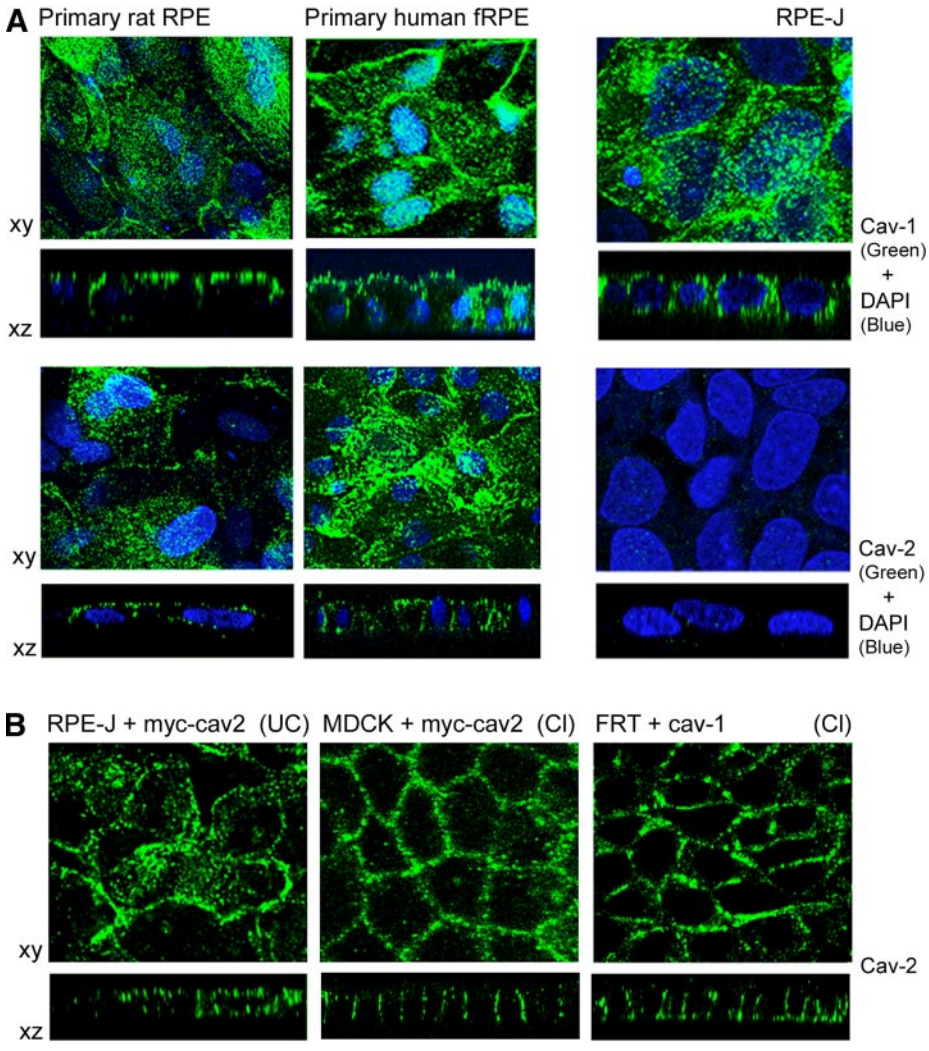

Fig. 3. *A*: immunohistochemical analysis of cav-1 and cav-2 distribution in cultured primary rat RPE, primary human fetal (f)RPE and in RPE-J cells. Cells were processed for immunofluorescence microscopy and stained with either a polyclonal anti-cav-1 antibody or a monoclonal antibody against cav-2. Nuclei stained with DAPI are blue. *B*: localization of overexpressed cav-2 in RPE-J cells and comparison with the distribution of this antigen in MDCK and FRT cells by immunostaining with a polyclonal anti-cav-2 antibody. UC, uncloned pool of RPE-J cells overexpressing human myc-tagged cav-2 (myc-cav2); Cl, clones of MDCK cells or FRT cells expressing ectopically human myc-cav-2 or cav-1, respectively. The confocal micrographs are representative horizontal or vertical scans in the *x-y* or *x-z* planes, respectively.

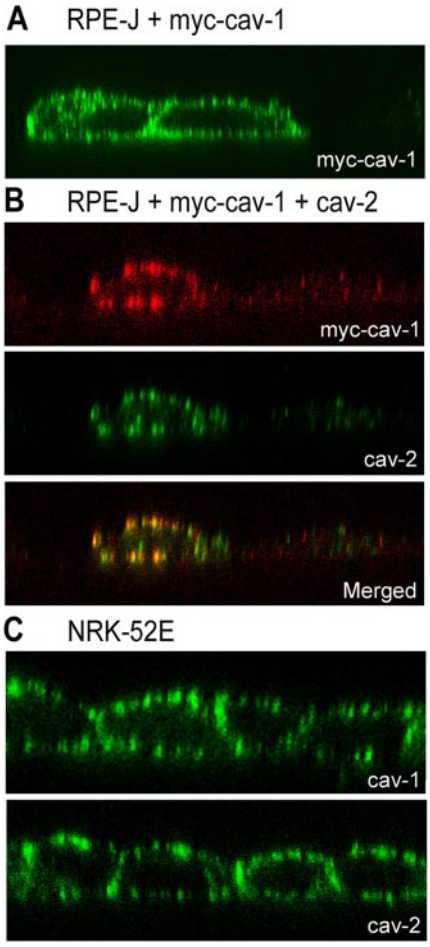

Fig. 4. Immunohistochemical localization of transiently overexpressed caveolins in RPE-J and of endogenous caveolins in NRK-52E cells. *A*: localization of transfected myc-cav-1 in RPE-J cells, using a polyclonal anti-myc antibody. *B*: RPE-J cells cotransfected with myc-cav-1 and nontagged cav-2. The double staining was performed with a monoclonal anti-myc antibody and a polyclonal anti-cav-2 antibody. Note that in cells ectopically coexpressing cav-1 and cav-2, the distribution of both these proteins is nonpolar and the two isoforms colocalize. *C*: immunohistochemical analysis of cav-1 and cav-2 distribution in NRK-52E cells stained with either a polyclonal anti-cav-1 or anti-cav-2 monoclonal antibody. The confocal micrographs are representative vertical scans in the *x-z* planes.

containing 3% BSA (TBSTA) blocking solution. The membranes were then probed with antibodies to caveolin-1 IgG and caveolin-2 in TBSTA. Signals were detected with appropriate horseradish peroxidase-coupled secondary antibodies, using either standard chemiluminescent (PerkinElmer Life Sciences, Boston, MA) or enhanced (Pierce Biotechnology) chemiluminescent (Femto-ECL) reagents.

Thin-Section Electron Microscopy

Eyes collected from the Long-Evans rat strain were fixed by intracardiac perfusion with 2% paraformaldehyde plus 1% glutaraldehyde in PBS/CM. The perfusion-fixed eyes were enucleated, the corneas were incised, and then further immersion fixed for 2 h in 0.1 M sodium cacodylate containing 2% glutaraldehyde and 4% paraformaldehyde. The rat eyes were then postfixed with 1% OsO_4 in 0.1 M cacodylate buffer, pH 7.4. After the eyes were dehydrated, en bloc stained with uranyl acetate, and embedded in Epon, 60- to 70-nm-thick sections were cut with the use of a diamond knife (Diatome, Fort Washington, PA). The specimens were stained with lead citrate, examined, and photographed at 80 kV with an electron microscope (model JEOL-100 CXII; Jeol, Peabody, MA).

Cells grown on polycarbonate Transwell R filters were processed for thin section electron microscopy by standard procedures as described previously (25). For quantitation of caveolae in RPE cells, cell segments from two different experiments (10 fields/experiment) were randomly photographed. Quantitative evaluations were carried out on micrographs printed at the same magnification (×28,000). Quantitation was performed with a NIH Image 1.52 program.

Preembedding Immunocytochemistry

Cells grown on 6.5 mm polycarbonate Transwell R filters were fixed in 3% paraformaldehyde (10 min, 37°C) and exposed to 0.1% Triton X-100 for 10 min at room temperature (24). They were then washed for 30 min in PBS containing 0.01 M glycine, 0.2% bovine serum albumin, 0.2% gelatine, and 5% normal goat serum (blocking buffer). For immunogold labeling, the cells were incubated with anti-caveolin-1 antibody (1:100), followed by 10-nm gold goat anti-rabbit IgG conjugate (1:20) (Ted Pella, Redding, CA). After being washed, the immune complexes were stabilized by fixation of cells for 30 min in 1% glutaraldehyde in 0.1 M cacodylate buffer, pH 7.4, and the filters further processed as described above for thin-section electron microscopy.

Evaluation of Biophysical Properties of Caveolins

Determination of such biophysical properties as *1*) flotation in discontinuous sucrose gradients and *2*) oligomerization state of caveolins were performed as described previously (6, 25, 28).

Detergent lysis and centrifugation to equilibrium on sucrose density gradients. Confluent cells (150 mm dishes) were lysed for 30 min in 2 ml of ice-cold TNE buffer (150 mM NaCl, 25 mM Tris·HCl, pH 7.5, and 5 mM EDTA) containing 1% Triton X-100, homogenized with a 23-gauge needle, followed by eight strokes in a loose-fitting Dounce homogenizer. The homogenate was adjusted to 60% sucrose and 4 ml of this sample was overlaid in a centrifuge tube with a discontinuous sucrose gradient (2 ml of 50% sucrose, 4 ml of 35% sucrose, 1 ml of 15% sucrose, and 0.6 ml of TNE buffer). The samples were centrifuged at 4°C for 20 h at 35,000 rpm in a SW41 rotor (Beckman Instruments). From the top of each gradient, 1-ml aliquots were harvested to yield a total of 12 fractions. An equal volume from each gradient fraction was separated by SDS-PAGE and subjected to immunoblot analysis.

Table 1. *Frequency of caveolae in RPE cells*

Cell Type	Localization	No. of Caveolae, per mm of Apical or Basolateral Membrane	%Total Caveolae
Rat RPE in situ	Apical	5	36
	Basolateral	9	64
Rat RPE-P	Apical	84	39.1
	Basolateral	131	60.9
Rat RPE-J	Apical	316	42.8
	Basolateral	422	57.2
Human f-RPE	Apical	63	35.4
	Basolateral	115	64.6
NRK-52E	Apical	1,168	59.5
	Basolateral	795	40.5
MDCK	Apical	3	0.3
	Basolateral	1,035	99.7

RPE, retinal pigment epithelium; NRK, normal rat kidney; f-RPE, fetal RPE; MDCK, Madin-Darby canine kidney. The number of caveolae on the cell surface was determined as described in the text. The data for MDCK cells, taken from Ref. 25, are shown for comparison.

Velocity gradient centrifugation. To estimate the oligomeric state of caveolins in RPE-J and MDCK cells, we used a previously described protocol (25, 28). Briefly, 0.5 ml of samples prepared in a solution composed of (in mM) 25 MES, pH 6.5, 150 NaCl, and 60 *N*-octyl β-D-glucopyranoside, were loaded upon a 5–50% linear sucrose gradient and centrifuged at 40,000 rpm for 16 h in a Beckman 50.1 rotor. Twelve gradient fractions were collected from the top, and equal aliquots from each fraction were subjected to immunoblot analysis. Molecular mass standards for velocity gradient centrifugation were as we described previously (25).

RESULTS

Nonpolar Localization of Caveolins-1 and -2 in Retinal Pigment Epithelium

Western blot analysis detected caveolins-1 and -2 in RPE collected from rat eyes at postnatal *days 2* and *22*, in primary cultures of rat RPE (rRPE-P) and human fetal RPE (hf-RPE) and in the RPE-J cell line (Fig. 1). For comparison, the presence of these proteins was investigated in several epithelial cell lines (NRK-52E, FRT, CaCo2, and MDCK) and in heart and brain (Fig. 1, *B* and *C*). Caveolin-1 was detected in RPE in situ at levels three to four times lower than in RPE-J cells (Fig. 1). Caveolin-2 was expressed roughly at similar levels in RPE in situ and in RPE-J cells (Fig. 1). Cloned RPE-J cells have five and two times less caveolin-1 than MDCK and NRK-52E, respectively (Fig. 1*B*). The level of caveolin-1 in rRPE-P and in RPE-J cells was approximately similar (Fig. 1*A*).

We performed immunofluorescence staining on frozen sections of RPE in situ to determine the localization of caveolins (Fig. 2). To mark the position of the RPE, we used an antibody to glucose transporter 1 (GLUT1), which displays a nonpolarized distribution in adult rat RPE (45) and therefore serves to delineate the apical and basolateral membranes of this epithelium. Cryosections of neural retina-free preparations of RPE-choroid were obtained (RPE at the top, choroid below) and were double immunolabeled with monoclonal antibodies against either caveolin-1 or -2 and a polyclonal antibody against GLUT1, followed by Alexa 594- and Alexa 488-conjugated secondary antibodies, respectively (Fig. 2, *A1–C4*; cell nuclei were stained blue with 4′,6-diamidino-2-phenylindole). Figure 2*A1* illustrates a typical example of the weak signal detected for caveolin-1 in RPE cells compared with the very strong staining observed in the choroid blood vessels (arrows in *A1*). By measuring the fluorescence intensity we estimate that the level of caveolin-1 in RPE in situ is roughly 10–12 times lower than in the choroid vessels. At higher magnification (Fig. 2*B1*), the comparison with the localization pattern of GLUT 1 clearly illustrates that caveolin-1 is present on both apical and basolateral membranes. The expression level of caveolin-2 (Fig. 2, *C1–C4*) in RPE in situ was below the detection limits of the monoclonal antibody used. Note that in control sections (Fig. 2, *A4* and *A5*), no specific staining was observed.

We detected intense immunofluorescence labeling of caveolin-1 in rRPE-P and hfRPE-P, as well as in immortalized RPE-J cells. In all cases, the caveolin-1 localization was not polarized (Fig. 3*A*). Caveolin-2 was detected with a nonpolar distribution in both rRPE-P cells and in hfRPE-P (Fig. 3*A*). In RPE-J cells, endogenous caveolin-2 was below detection levels but exogenous myc-tagged caveolin-2 displayed a nonpolar distribution (Fig. 3*B*). By contrast, the subcellular localization of myc-caveolin-2 in MDCK cells is basolateral (Fig. 3*B*) (25). Similarly, the distribution of endogeneous caveolin-2 is basolateral in FRTcells expressing exogenous caveolin-1 (Fig. 3*B*), whereas wild-type FRT cells, which lack caveolin-1, localize caveolin-2 to the Golgi complex (data not shown, see Ref. 25).

Overexpression of either caveolin-2 or caveolin-1, and both caveolin-1 and caveolin-2, did not affect the nonpolar distribution of these proteins in RPE-J cells (Fig. 3*B* and Fig. 4, *A* and *B*). These data indicate that the nonpolar localization of caveolin-2 is not related to the reduced levels of caveolins 1

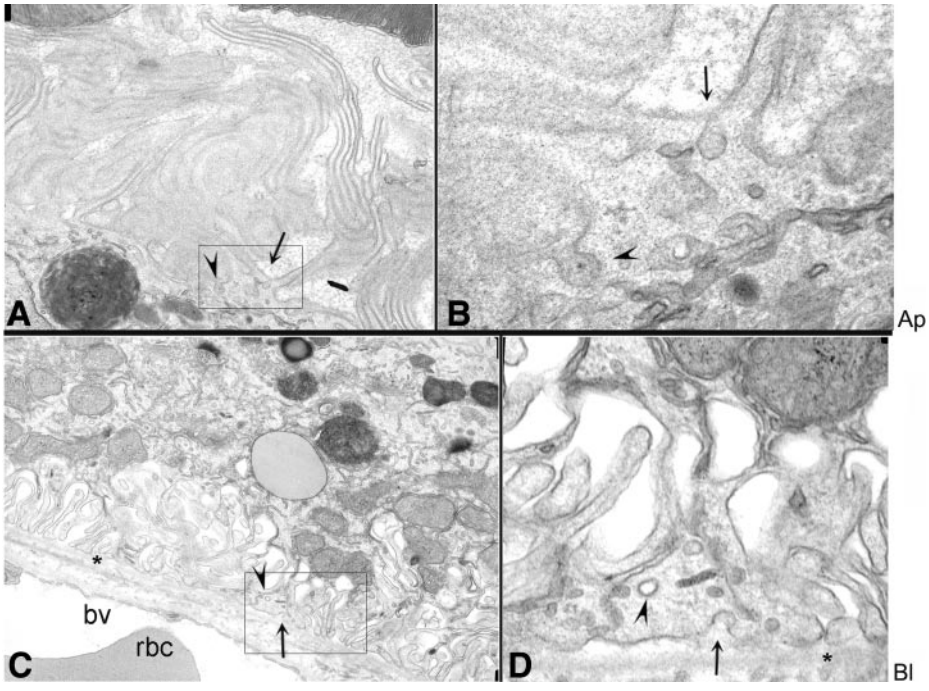

Fig. 5. Analysis of caveolae in intact retina of an adult rat. Representative electron micrographs show that the occasionally seen plasmalemmal caveolae were distributed on both apical (Ap; *A* and *B*) and basolateral (Bl) plasmalemma (*C* and *D*). *B*: higher magnification of a typical, flasked-shaped caveolar structure (arrow), assembled at the base of microvilli. A nearby coated vesicle is indicated by an arrowhead. An omega-shaped, open caveola (arrow) on the basolateral membrane near a coated vesicle (arrowhead) is shown in *C* and *D*. *B* and *D* are higher magnifications of the areas framed in *A* and *C*, respectively. bv, blood vessel, rbc, red blood cell, *basal lamina. *A*, ×18,000; *B*, ×70,000; *C*, ×13,000; and *D*, ×51,000.

and/or caveolin-2 in RPE-J cells compared with MDCK cells but rather to other unknown cell-specific factors.

In addition, we examined the distribution of caveolins in the epithelioid cell line NRK-52E, which also expresses lower levels of caveolin-1 relative to MDCK cells but higher levels of caveolin-2 than RPE-J cells (Fig. 1*B*). As shown in Fig. 4*C*, we found that in NRK-52E both caveolin-1 and caveolin-2 are nonpolarly distributed, similar to RPE cells. Significantly, overexpression of either caveolin-1 or caveolin-2 in NRK cells did not change the nonpolarized distribution of these proteins (data not shown). Because the distribution of endogenous (19) and exogenous (Fig. 3*B*) caveolin-2 is basolateral in MDCK cells and the nonpolarized distribution of caveolin-2 is maintained both in RPE-J and NRK-52E cells by increasing caveolin expression levels, we conclude that the above data are consistent with a cell-specific localization and polarity of caveolin-2.

Nonpolar Assembly of Caveolae in RPE: Electron Microscopic Analysis

Table 1 summarizes the quantitation of plasmalemmal caveolae in the various RPE cell types, as examined by transmission electron microscopy. Representative electron micrographs of all RPE cell types in this study are shown in Figs. 5, 6, 7,and 8. Caveolae were rare in rat RPE in situ but were easily detected in rRPE-P, hfRPE-P, and RPE-J cells. Compared with MDCK cells (25), cultured RPE cells displayed 20 to 25 times higher density of apical caveolae and 10–40% lower density of basolateral caveolae. Typical omega-shaped structures with or without single-layered stomatal diaphragms are present on both the apical and basolateral plasmalemma in all RPE cells examined: rat RPE in situ (Fig. 5), rRPE-P (Fig. 6, *IA–IC*) and hfRPE-P (Fig. 8) as well as in RPE-J cell line (Fig. 6*II*). The size of apical plamalemmal caveolae in RPE-J

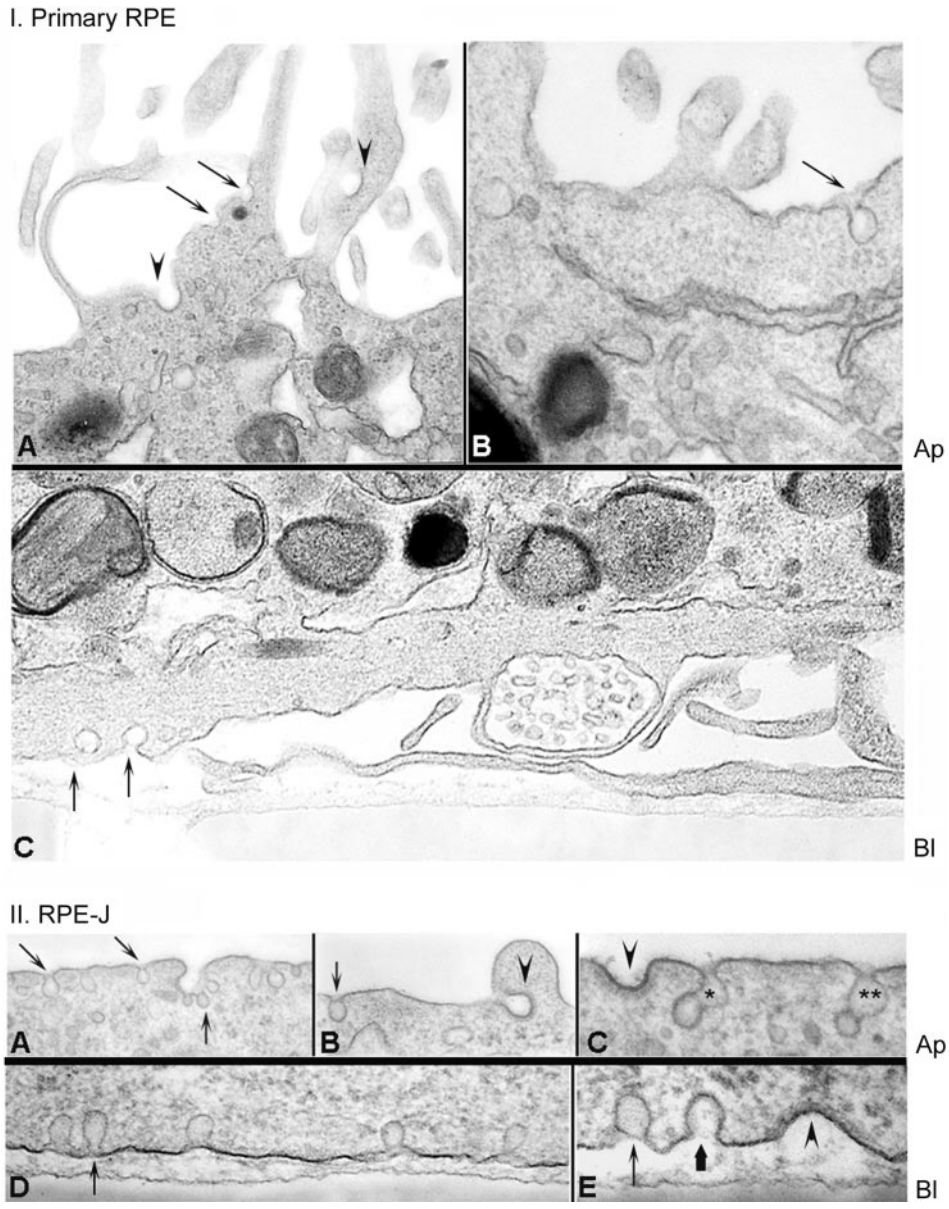

Fig. 6. Analysis of caveolae in primary rat RPE and RPE-J cells. Electron micrographs depicting nonpolar distribution of caveolae (arrows) both in primary rat RPE (*I*) and confluent monolayers of RPE-J cells (*II*) grown on polycarbonate filters. (*I*) illustrates the typical caveolar structures with open stomata (*IA*) or sharply bent rims (*IB* and *IC*) found in primary RPE cells. In (*II*) are shown characteristic plasmalemmal caveolae found in RPE-J cells: clusters of caveolae into racemose structures (*IIA*), caveolae with single-layered stomatal diaphragm (*IIB*) and caveolae with elongated and narrow neck (*IID*). Note the particular tubular structures in (*IIC*) apparently formed by fused plasmalemmal caveolae (*,**). The caveolar tubules shown in IIC display fine stomatal diaphragms between the two fused vesicles (*,**) as well as on the vesicle connected to the plasmalemma (**). *IIE* is a higher magnification showing typical caveolar structure on the basolateral membrane either with (arrow) or without a diaphragm (large arrow); see the nearby clathrin-coated pit (arrowhead). *IA*, ×39,000; *IB*, ×68,000; *IC*, ×45,000; *IIA*, ×33,000; *IIB*, ×39,000; *IIC*, ×72,000; *IID*, ×64,000; *IIE*, ×93,000.

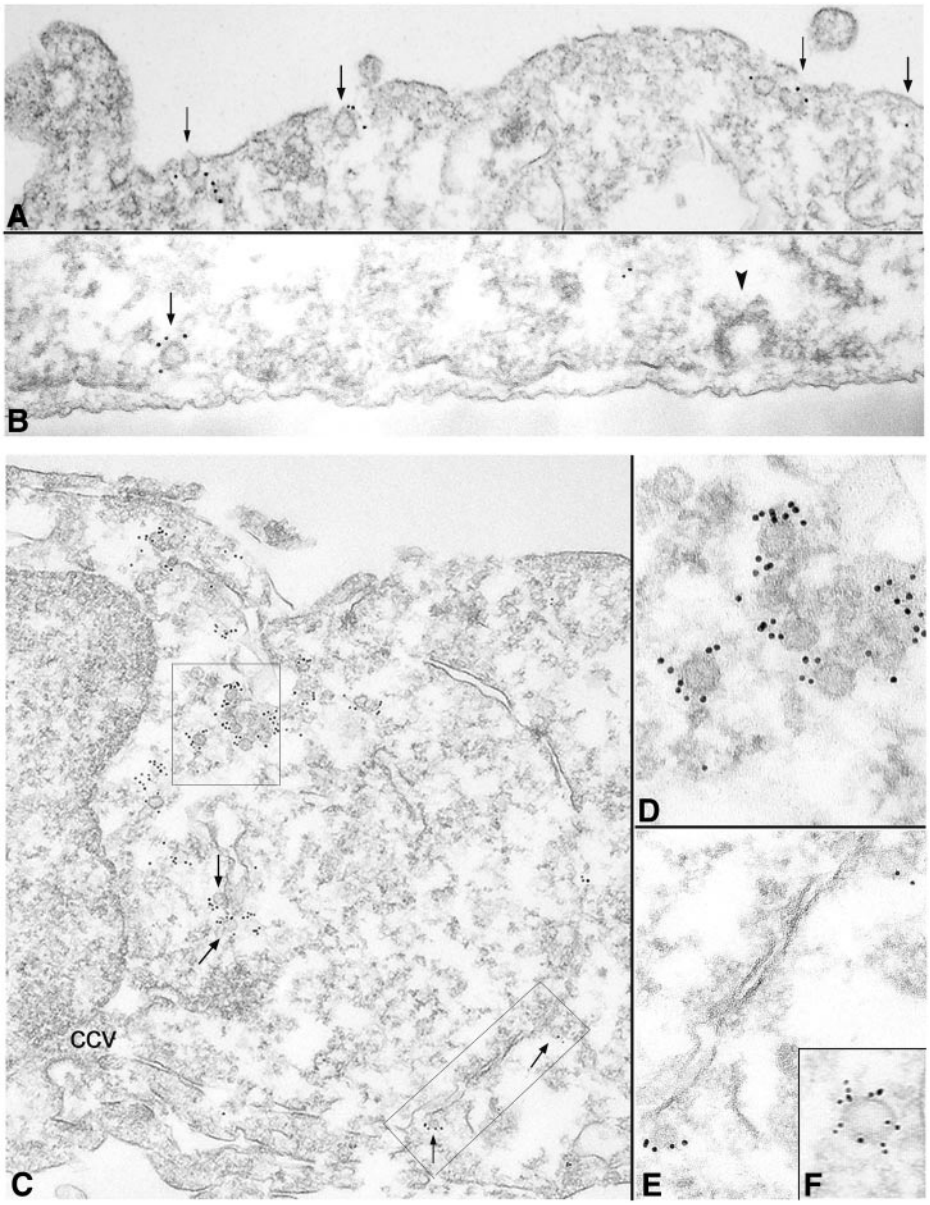

Fig. 7. Immunogold localization of cav-1 to caveolae in RPE-J cells. Gold particles (arrows) can be seen along uncoated, omega-shaped caveolar structures at both apical (*A*) and basolateral (*B*) plasma membranes but not on clathrin-coated vesicles (CCV; arrowhead). *C*: the cav-1 gold particles are also decorating intracellularly located caveolar membranes. *D* and *E*: higher magnifications of the framed areas shown in *C*. *F*, *inset*: on some vesicles, the gold particles appear to be aligned radially on caveolae. *A*, ×62,000; *B*, ×86,000; *C*, ×36,000; *D*, ×99,000; *E*, ×98,000; and *F*, ×108,000.

cells was more heterogeneous (50–90 nm in diameter) than that of basolateral caveolae (60–70 nm in diameter). Occasionally in RPE-J cells, chains of two fused caveolar vesicles were noticed (Fig. 6*IIC*; asterisks). These caveolar "tubules" (Fig. 6*IIC*) had fine stomatal diaphragms between the two fused vesicles as well as on the vesicle connected to the plasmalemma.

Immunogold electron microscopy in RPE-J cells demonstrated that caveolar structures on both the apical and basolateral plasmalemma (Fig. 7, *A*, *B*, *D*, and *E*), as well as in the cytoplasm, were specifically labeled by caveolin-1 antibody (Fig. 7*C*). In some favorable sections the immunogold-tagged caveolin antibody decorated caveolar structures radially, along short virtual filaments of 20–22 nm in length (Fig. 7*F*).

Notably, similar to the RPE cell lines, in the epithelioid NRK-52E cells, we also found a nonpolar distribution of caveolae (Table 1).

Biophysical Properties of Caveolins in RPE Cells

Flotation and oligomerization assay. When a Triton lysate of RPE-J cells was analyzed with the use of a buoyant equilibrium sucrose density gradient (Fig. 9*A*, raft flotation assay), a fraction of the caveolin in RPE-J cells floated to a low-density position in the gradient (*fractions 1–3* in the centrifuge tube). This result is similar with that found for MDCK cells, where the caveolin-rich raft structure is typically distributed to the low-buoyant membrane microdomain fraction, shown as a control in Fig. 9*A*.

Oligomerization of caveolin is considered important for the biogenesis of caveolae, (9) as well as for its raft association and Golgi exit (34). By density gradient ultracentrifugation, caveolins in RPE-J cells were found in oligomeric complexes of similar size (200–670 kDa) to those found in MDCK cells (Fig. 9*B*, oligomerization assay).

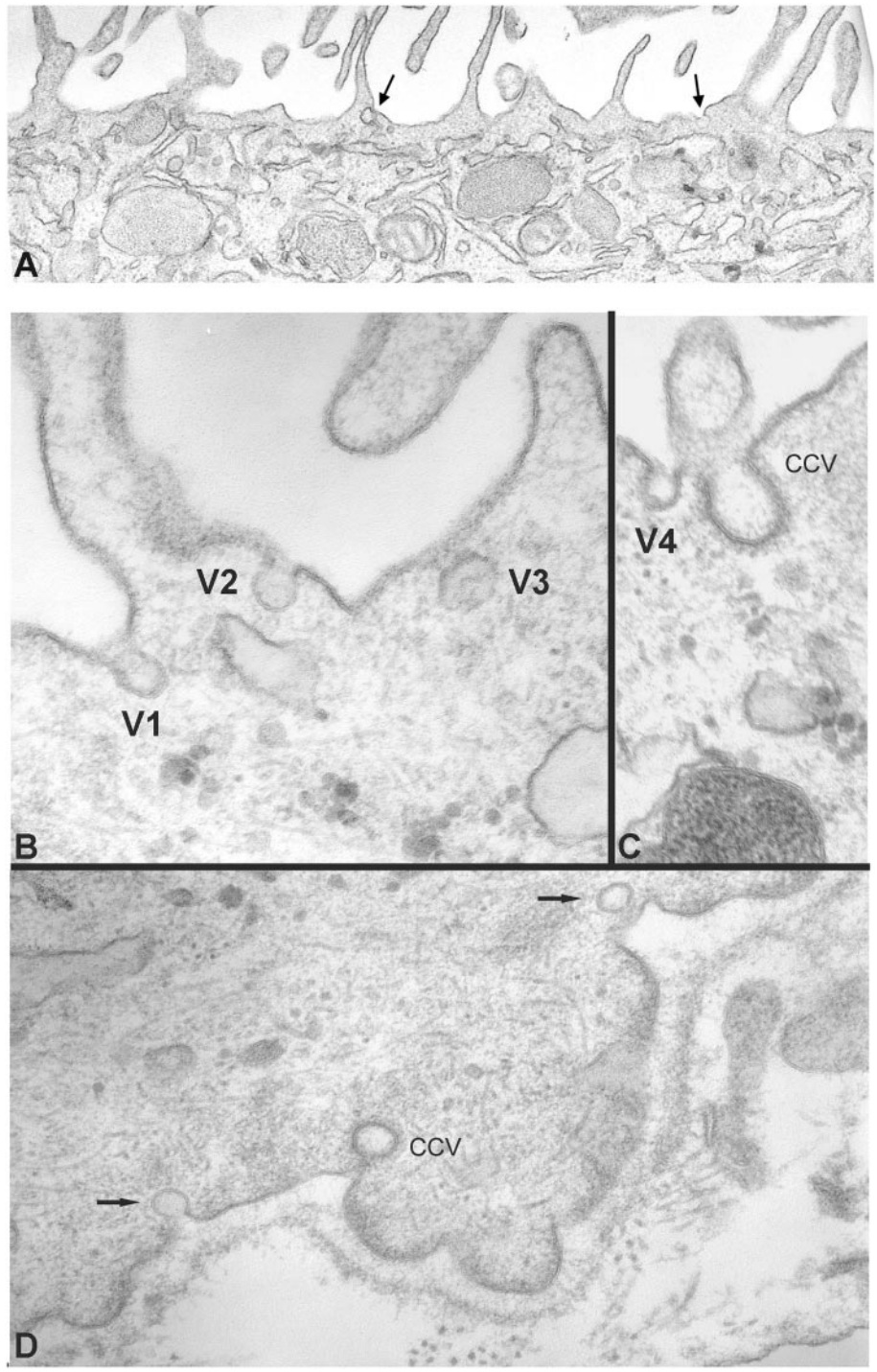

Fig. 8. Analysis of caveolae in primary human fetal RPE. *A*: low-magnification electron micrograph showing an apical area with caveolae (arrows) present on the planar plasmalemma separating microvilli or at the base of microvilli. *B*: at higher magnification the typical ultrastructural caveolar structures assembled on the two sides of a microvilus are shown (V1–V3); one of the caveolae has a characteristic constricted stoma (mouth) covered by a fine diaphragm (V1). *C*: the sizes of caveolae (V4) are smaller than those of CCV. *D*: the basolateral plasmalemma also displays characteristic smooth-surfaced caveolae (arrows), which are smaller-sized than the CCV. *A*, ×28,000; *B*, ×83,000; *C*, ×87,000; and *D*, ×64,000.

DISCUSSION

The most striking finding reported here is that RPE cells express caveolae at both apical and basolateral membranes. RPE in vivo displayed occasional caveolae on both apical and basolateral membranes but the surface density of plasmalemmal caveolae increased dramatically at both apical and basolateral plasma membrane domains in cultured primary rat and human RPE and in immortalized rat RPE-J cells. The electron microscopy results on the presence and localization of caveolae correlated well with our caveolin expression and localization data. The data presented here demonstrate expression of caveolins, in rat RPE in situ, primary cultures of rat RPE, human fetal RPE, and in the immortalized RPE-J cell line. In agreement with a previous study in mouse RPE (5), caveolin-1 was present in all three rat RPE cell types examined; however, these investigators did not report the presence of caveolae in mouse RPE and in ARPE-19 cells. By immunofluorescence the expression level of caveolin-1 in the rat RPE in situ was 10–12 times less than in adjacent blood vessels from the choroid. Compared with RPE in situ using

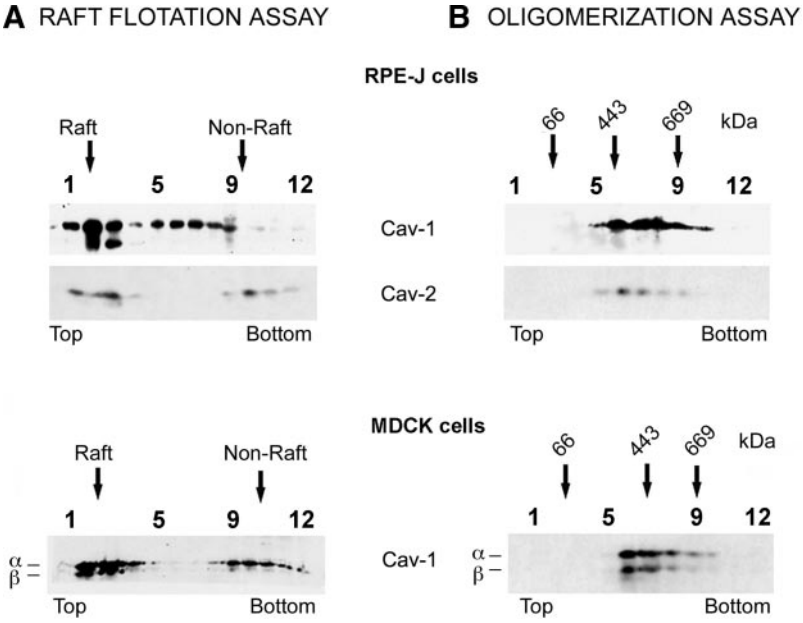

Fig. 9. Biophysical properties of caveolins. *A*: caveolins partition to low buoyant-density membrane fractions after flotation equilibrium sucrose density gradient ultracentrifugation. RPE-J cells were homogenized in a buffer containing 1% Triton X-100 and subjected to ultracentrifugation to equilibrium in sucrose density gradients. Twelve 1-ml fractions were collected from the top of the tube and aliquots from each fraction were analyzed by SDS-PAGE and Western blotting. The caveolar raft membrane fractions are enriched in *fractions 1–3*. *B*: velocity gradient ultracentrifugation for estimation of the oligomeric state of caveolins. RPE-J cells were solubilized, loaded atop a 0–50% sucrose density gradient, and subjected to centrifugation. Twelve fractions were recovered, starting from the top of the tube, and aliquots from each fraction were analyzed by SDS-PAGE and Western blotting. Caveolins in RPE-J were visualized using an enhanced chemiluminescent (Femto-ECL) kit and in MDCK cells were detected using a standard chemiluminescent system.

Western blot analysis, the levels of caveolin-1 in primary cultures of rat RPE and in RPE-J cell line were upregulated three to four times, which correlated very well with the increased numbers of caveolae at the plasma membrane.

The nonpolarized assembly of caveolae in RPE cells unraveled an interesting difference between RPE and other columnar epithelial cells, which assemble caveolae preferentially at the basolateral membrane. Interestingly, caveolin-1 and caveolin-2 were found to have a nonpolar distribution in RPE cells, consistent with the observation that caveolin-2 expression may be necessary in certain cells for the efficient assembly of plasmalemmal caveolae (19, 42). Thus, in MDCK cells, which express nonpolar caveolin-1 and basolateral caveolin-2 (25, 37), caveolar assembly is basolateral and efficient (19, 25, 49). In thyroid FRT cells, which lack caveolin-1, caveolin-2 expression is restricted to the Golgi complex, but transfection of caveolin-1 results in basolateral recruitment of caveolin-2 and efficient assembly of basolateral caveolae (25). By contrast, expression of caveolin-1 in CaCo2 cells, which lack caveolin-2, promotes the assembly of 6–10 times less caveolae than in MDCK cells (49). Remarkably, in this study, we also found that in MDCK and NRK-52E cell lines representing the distal and proximal renal tubular cells, respectively, the assembly of plasmalemmal caveolae is distinct. Thus, similar to RPE, in NRK-52E, the bipolar assembly of plasmalemmal caveolae also correlated with the nonpolar distribution of both caveolin-1 and 2. Therefore, our data for the two different epithelial cells (RPE and NRK-52E) provide additional support for the role of caveolin-2 in the polarized biogenesis of caveolae (19).

The mechanisms responsible for the cell-specific localization and polarity of caveolin-2 are not known. Identification of these mechanisms may help understand the nonpolarized distribution of caveolae in RPE cells and the polarized assembly of caveolae in other epithelial cells.

Another epithelial cell type, in which caveolae have a nonpolarized plasma membrane distribution, is the endothelial cell; in these cells, caveolae are involved in a dynamic transendothelial movement of serum molecules (27, 32, 43). In epithelial cells that assemble caveolae on the basolateral membrane, apical caveolae may be induced by some experimental conditions. Thus MDCK cells assembled apical caveolae when clustering of glycosyl phosphatidyl inositol (GPI)-anchored proteins was induced by antibodies to these proteins (48). Interestingly, the actin-depolymerizing drug cytochalasin D induced accumulation of both coated and noncoated apical membrane invaginations on the apical pole of the pancreatic acinar cells, as well as concomitant relocation of caveolin-1 from an intracellular compartment to the apical plasmalemma (46). These experiments suggest that the assembly of apical caveolae in RPE cells may be promoted by a different organization of the actin cytoskeleton in RPE or by a different organization (increased apical clustering?) of GPI-anchored proteins in this epithelium.

The presence of caveolin-2 at the apical membrane of RPE cells could reflect an altered intracellular sorting of caveolins. Previous work with permeabilized MDCK cells has shown that caveolin-1 homooligomers preferentially associate with nascent apical vesicles at the TGN, whereas caveolin-1/caveolin-2 heterooligomers associate with nascent basolateral vesicles (37). It has been suggested that this may reflect a role for caveolin-1 oligomers in regulating the route to the apical membrane and a role for caveolin-1/caveolin-2 heterooligomers in regulating the basolateral route. Perhaps RPE cells can form caveolin-1/caveolin-2 heterooligomers in the TGN but lack the ability to form caveolin-1 homooligomers. Alternatively, they might lack a factor (e.g., a kinase) that prevents the assembly of caveolin-1/caveolin-2 heterooligomers in the apical route of other epithelial cells (21). Any of these two scenarios could result in the "invasion" of the apical route by caveolin-2 and the consequent appearance of caveolin-2 at the apical surface. Furthermore, as caveolin-1 has been implicated in the exit of some plasma membrane proteins from the Golgi complex (25, 28, 41, 54), a differential assembly of caveolin oligomers at the Golgi complex could explain the altered pathway of the apical protein influenza HA, which follows a

transcytotic route via the basolateral membrane in RPE cells, but instead utilizes a direct route in MDCK cells.

The presence of apical caveolae could also reflect the presence of novel endocytic pathways in RPE cells, absent in other epithelial cells. Recent work (29) has identified a caveosome pathway that plays a key role in the internalization of SV40 from the plasma membrane. An alternative view is that caveolin-1 might act not as a determinant of caveolae invagination and internalization but rather as a regulator that stabilizes caveolae at the plasma membrane and reduces the endocytic potential of caveolae/raft domains (20). Finally, although low levels of caveolins in RPE in situ may not allow the existence of significant caveolar endocytic pathways, they might, however, be important for signaling events (22, 33). The low level of caveolins in RPE in situ might be related to the low proliferative potential of RPE in situ. Because caveolar levels have been found to be increased in certain cancers (51) and in certain proliferating cells (55), it may be interesting in the future to study the expression of caveolins in proliferative vitroretinopathy, a proliferative RPE disease.

In conclusion, RPE cells contain low levels of caveolin-1 and -2 compared with MDCK epithelial cells and display a nonpolar distribution of caveolae, probably due to the expression of caveolin-1 and caveolin-2 at both apical and basolateral membranes. The differences in their levels of expression and in their posttranslational modifications as well as their distinct localization pattern in different epithelial cell lines might modulate specialized sorting and trafficking phenotypes in different epithelial cell types. The molecular functions of caveolins in RPE remain to be clarified in future work.

GRANTS

This work was supported by National Eye Institute Grants EY-8538 (to E. Rodriguez-Boulan), EY-00444, and EY-00331 (to D. Bok), a Jules and Doris Stein Professorship from the Research to Prevent Blindness Foundation (to E. Rodriguez-Boulan), the Dolly Green Chair in Ophthalmology at UCLA (to D. Bok), and the Dyson Foundation.

REFERENCES

1. **Boesze-Battaglia K, Dispoto J, and Kahoe MA.** Association of a photoreceptor-specific tetraspanin protein, ROM-1, with Triton X-100-resistant membrane rafts from rod outer segment disk membranes. *J Biol Chem* 277: 41843–41849, 2002.
2. **Bonilha VL, Marmorstein AD, Cohen-Gould L, and Rodriguez-Boulan E.** Apical sorting of influenza hemagglutinin by transcytosis in retinal pigment epithelium. *J Cell Sci* 110: 1717–1727, 1997.
3. **Bosch E, Horwitz J, and Bok D.** Phagocytosis of outer segments by retinal pigment epithelium: phagosome-lysosome interaction. *J Histochem Cytochem* 41: 253–263, 1993.
4. **Breton S, Lisanti MP, Tyszkowski R, McLaughlin M, and Brown D.** Basolateral distribution of caveolin-1 in the kidney. Absence from H^+-ATPase-coated endocytic vesicles in intercalated cells. *J Histochem Cytochem* 46: 205–214, 1998.
5. **Bridges CC, El-Sherbeny A, Roon P, Ola MS, Kekuda R, Ganapathy V, Camero RS, Cameron PL, and Smith SB.** A comparison of caveolae and caveolin-1 to folate receptor alpha in retina and retinal pigment epithelium. *Histochem J* 33: 149–158, 2001.
6. **Brown DA and Rose JK.** Sorting of GPI-anchored proteins to glycolipid-enriched membrane subdomains during transport to the apical cell surface. *Cell* 68: 533–544, 1992.
7. **Calvo M, Tebar F, Lopez-Iglesias C, and Enrich C.** Morphologic and functional characterization of caveolae in rat liver hepatocytes. *Hepatology* 33: 1259–1269, 2001.
8. **Elliott MH, Fliesler SJ, and Ghalayini AJ.** Cholesterol-dependent association of caveolin-1 with the transducin alpha subunit in bovine photoreceptor rod outer segments: disruption by cyclodextrin and guanosine 5′-O-(3-thiotriphosphate). *Biochemistry* 42: 7892–7903, 2003.
9. **Fernandez I, Ying Y, Albanesi J, and Anderson RG.** Mechanism of caveolin filament assembly. *Proc Natl Acad Sci USA* 99: 11193–11198, 2002.
10. **Fra AM, Williamson E, Simons K, and Parton RG.** De novo formation of caveolae in lymphocytes by expression of VIP21-caveolin. *Proc Natl Acad Sci USA* 92: 8655–8659, 1995.
11. **Fujimoto T, Kogo H, Nomura R, and Une T.** Isoforms of caveolin-1 and caveolar structure. *J Cell Sci* 113: 3509–3517, 2000.
12. **Galbiati F, Razani B, and Lisanti MP.** Emerging themes in lipid rafts and caveolae. *Cell* 106: 403–411, 2001.
13. **Gundersen D, Orlowski J, and Rodriguez-Boulan E.** Apical polarity of Na,K-ATPase in retinal pigment epithelium is linked to a reversal of the ankyrin-fodrin submembrane cytoskeleton. *J Cell Biol* 112: 863–872, 1991.
14. **Gundersen D, Powell SK, and Rodriguez-Boulan E.** Apical polarization of N-CAM in retinal pigment epithelium is dependent on contact with the neural retina. *J Cell Biol* 121: 335–343, 1993.
15. **Hu J and Bok D.** A cell culture medium that supports the differentiation of human retinal pigment epithelium into functionally polarized monolayers. *Mol Vis* 7: 14–19, 2001.
16. **Hu JG, Gallemore RP, Bok D, Lee AY, and Frambach DA.** Localization of Na-K-ATPase on cultured human retinal pigment epithelium. *Invest Ophthalmol Vis Sci* 35: 3582–3588, 1994.
17. **Isshiki M, Ying YS, Fujita T, and Anderson RG.** A molecular sensor detects signal transduction from caveolae in living cells. *J Biol Chem* 277: 43389–43398, 2002.
18. **Kogo H, Aiba T, and Fujimoto T.** Cell type-specific occurrence of caveolin-1α and -1β in the lung caused by expression of distinct mRNAs. *J Biol Chem* 279: 25574–25581, 2004.
19. **Lahtinen U, Honsho M, Parton RG, Simons K, and Verkade P.** Involvement of caveolin-2 in caveolar biogenesis in MDCK cells. *FEBS Lett* 538: 85–88, 2003.
20. **Le PU, Guay G, Altschuler Y, and Nabi IR.** Caveolin-1 is a negative regulator of caveolae-mediated endocytosis to the endoplasmic reticulum. *J Biol Chem* 277: 3371–3379, 2002.
21. **Lee H, Park DS, Wang XB, Scherer PE, Schwartz PE, and Lisanti MP.** Src-induced phosphorylation of caveolin-2 on tyrosine 19. Phosphocaveolin-2 [Tyr(P)19] is localized near focal adhesions, remains associated with lipid rafts/caveolae, but no longer forms a high molecular mass hetero-oligomer with caveolin-1. *J Biol Chem* 277: 34556–34567, 2002.
22. **Liu P, Rudick M, and Anderson RG.** Multiple functions of caveolin-1. *J Biol Chem* 277: 41295–41298, 2002.
23. **Marmorstein AD, Gan YC, Bonilha VL, Finnemann SC, Csaky KG, and Rodriguez-Boulan E.** Apical polarity of N-CAM and EMMPRIN in retinal pigment epithelium resulting from suppression of basolateral signal recognition. *J Cell Biol* 142: 697–710, 1998.
24. **Moldovan NI, Heltianu C, Simionescu N, and Simionescu M.** Ultrastructural evidence of differential solubility in Triton X-100 of endothelial vesicles and plasma membrane. *Exp Cell Res* 219: 309–313, 1995.
25. **Mora R, Bonilha VL, Marmorstein A, Scherer PE, Brown D, Lisanti MP, and Rodriguez-Boulan E.** Caveolin-2 localizes to the golgi complex but redistributes to plasma membrane, caveolae, and rafts when co-expressed with caveolin-1. *J Biol Chem* 274: 25708–25717, 1999.
26. **Palade GE.** Fine structure of blood capillaries. *J Appl Physiol* 24: 1424–1436, 1953.

25a. **Nabi IR, Mathews AP, Cohen-Gould L, Gundersen D, and Rodriguez-Boulan E.** Immortalization of polarized rat retinal pigment epithelium. *J Cell Sci* 104: 37–49, 1993.

27. **Palade GE and Bruns RR.** Structural modulations of plasmalemmal vesicles. *J Cell Biol* 37: 633–649, 1968.
28. **Parolini I, Sargiacomo M, Galbiati F, Rizzo G, Grignani F, Engelman JA, Okamoto T, Ikezu T, Scherer PE, Mora R, Rodriguez-Boulan E, Peschle C, and Lisanti MP.** Expression of caveolin-1 is required for the transport of caveolin-2 to the plasma membrane. Retention of caveolin-2 at the level of the golgi complex. *J Biol Chem* 274: 25718–25725, 1999.
29. **Pelkmans L, Burli T, Zerial M, and Helenius A.** Caveolin-stabilized membrane domains as multifunctional transport and sorting devices in endocytic membrane traffic. *Cell* 118: 767–780, 2004.
30. **Pelkmans L and Helenius A.** Endocytosis via caveolae. *Traffic* 3: 311–320, 2002.
31. **Philp NJ, Yoon H, and Grollman EF.** Monocarboxylate transporter MCT1 is located in the apical membrane and MCT3 in the basal membrane of rat RPE. *Am J Physiol Regul Integr Comp Physiol* 274: R1824–R1828, 1998.

32. **Predescu D, Vogel SM, and Malik AB.** Functional and morphological studies of protein transcytosis in continuous endothelia. *Am J Physiol Lung Cell Mol Physiol* 287: L895–L901, 2004.
33. **Razani B, Woodman SE, and Lisanti MP.** Caveolae: from cell biology to animal physiology. *Pharmacol Rev* 54: 431–467, 2002.
34. **Ren X, Ostermeyer AG, Ramcharan LT, Zeng Y, Lublin DM, and Brown DA.** Conformational defects slow Golgi exit, block oligomerization, and reduce raft affinity of caveolin-1 mutant proteins. *Mol Biol Cell* 15: 4556–4567, 2004.
35. **Rodriguez-Boulan E, Kreitze G, and Musch A.** Organization of vesicular trafficking in epithelia. *Nat Rev Mol Cell Biol* 6: 233–247, 2005.
36. **Rothberg KG, Heuser JE, Donzell WC, Ying YS, Glenney JR, and Anderson RG.** Caveolin, a protein component of caveolae membrane coats. *Cell* 68: 673–682, 1992.
37. **Scheiffele P, Verkade P, Fra AM, Virta H, Simons K, and Ikonen E.** Caveolin-1 and -2 in the exocytic pathway of MDCK cells. *J Cell Biol* 140: 795–806, 1998.
38. **Scherer PE, Lewis RY, Volonte D, Engelman JA, Galbiati F, Couet J, Kohtz DS, van Donselaar E, Peters P, and Lisanti MP.** Cell-type and tissue-specific expression of caveolin-2. Caveolins 1 and 2 co-localize and form a stable hetero-oligomeric complex in vivo. *J Biol Chem* 272: 29337–29346, 1997.
39. **Shin JS, Gao Z, and Abraham SN.** Involvement of cellular caveolae in bacterial entry into mast cells. *Science* 289: 785–788, 2000.
40. **Song KS, Scherer PE, Tang Z, Okamoto T, Li S, Chafel M, Chu C, Kohtz DS, and Lisanti MP.** Expression of caveolin-3 in skeletal, cardiac, and smooth muscle cells. Caveolin-3 is a component of the sarcolemma and co-fractionates with dystrophin and dystrophin-associated glycoproteins. *J Biol Chem* 271: 15160–15165, 1996.
41. **Sotgia F, Razani B, Bonuccelli G, Schubert W, Battista M, Lee H, Capozza F, Schubert AL, Minetti C, Buckley JT, and Lisanti MP.** Intracellular retention of glycosylphosphatidyl inositol-linked proteins in caveolin-deficient cells. *Mol Cell Biol* 22: 3905–3926, 2002.
42. **Sowa G, Pypaert M, Fulton D, and Sessa WC.** The phosphorylation of caveolin-2 on serines 23 and 36 modulates caveolin-1-dependent caveolae formation. *Proc Natl Acad Sci USA* 100: 6511–6516, 2003.
43. **Stan RV.** Structure and function of endothelial caveolae. *Microsc Res Tech* 57: 350–364, 2002.
44. **Thomsen P, Roepstorff K, Stahlhut M, and van Deurs B.** Caveolae are highly immobile plasma membrane microdomains, which are not involved in constitutive endocytic trafficking. *Mol Biol Cell* 13: 238–250, 2002.
45. **Tserentsoodol N, Shin BC, Suzuki T, and Takata K.** Colocalization of tight junction proteins, occludin and ZO-1, and glucose transporter GLUT1 in cells of the blood-ocular barrier in the mouse eye. *Histochem Cell Biol* 110: 543–551, 1998.
46. **Valentijn KM, Gumkowski FD, and Jamieson JD.** The subapical actin cytoskeleton regulates secretion and membrane retrieval in pancreatic acinar cells. *J Cell Sci* 112: 81–96, 1999.
47. **Vallejo J and Hardin CD.** Expression of caveolin-1 in lymphocytes induces caveolae formation and recruitment of phosphofructokinase to the plasma membrane. *FASEB J* 00: 000–000, 2005.
48. **Verkade P, Harder T, Lafont F, and Simons K.** Induction of caveolae in the apical plasma membrane of Madin-Darby canine kidney cells. *J Cell Biol* 148: 727–739, 2000.
49. **Vogel U, Sandvig K, and van Deurs B.** Expression of caveolin-1 and polarized formation of invaginated caveolae in Caco-2 and MDCK II cells. *J Cell Sci* 111: 825–832, 1998.
50. **Way M and Parton RG.** M-caveolin, a muscle-specific caveolin-related protein. *FEBS Lett* 376: 108–112, 1995.
51. **Williams TM, Hassan GS, Li J, Cohen AW, Medina F, Frank PG, Pestell RG, Di Vizio D, Loda M, and Lisanti MP.** Caveolin-1 promotes tumor progression in an autochthonous mouse model of prostate cancer: genetic ablation of Cav-1 delays advanced prostate tumor development in tramp mice. *J Biol Chem* 280: 25134–25145, 2005.
52. **Williams TM and Lisanti MP.** The caveolin genes: from cell biology to medicine. *Ann Med* 36: 584–595, 2004.
53. **Williams TM and Lisanti MP.** Caveolin-1 in oncogenic transformation, cancer, and metastasis. *Am J Physiol Cell Physiol* 288: C494–C506, 2005.
54. **Wyse BD, Prior IA, Qian H, Morrow IC, Nixon S, Muncke C, Kurzchalia TV, Thomas WG, Parton RG, and Hancock JF.** Caveolin interacts with the angiotensin II type 1 receptor during exocytic transport but not at the plasma membrane. *J Biol Chem* 278: 23738–23746, 2003.
55. **Yokomori H, Oda M, Wakabayashi G, Kitajima M, Yoshimura K, Nomura M, and Hibi T.** High expressions of caveolins on the proliferating bile ductules in primary biliary cirrhosis. *World J Gastroenterol* 11: 3710–3713, 2005.
56. **Young RW and Bok D.** Participation of the retinal pigment epithelium in the rod outer segment renewal process. *J Cell Biol* 42: 392–403, 1969.